MOLECULAR DYNAMIC SIMULATION OF ZIGZAG SILICON CARBIDE NANORIBBON

HANG T. T. NGUYEN[1,2,†]

[1]*Laboratory of Computational Physics, Faculty of Applied Science,*
Ho Chi Minh City University of Technology (HCMUT), Ho Chi Minh City,
268 Ly Thuong Kiet Street, District 10, Ho Chi Minh City, Vietnam
[2]*Vietnam National University Ho Chi Minh City,*
Linh Trung Ward, Thu Duc District, Ho Chi Minh City, Vietnam

E-mail: [†]hangbk@hcmut.edu.vn

Abstract. *The heating process of zigzag silicon carbide nanoribbon (SiCNR) is studied via molecular dynamics (MD) simulation. The initial model contained 10000 atoms is heating from 50 K to 5000 K to study the structural evolution of zigzag SiCNR. The melting point is defined at 4010 K, the phase transition from solid to liquid exhibits the first-order type. The mechanism of structural evolution upon heating is studied based on the radial distribution functions, coordination number, ring distributions, and angle distributions.*

Keywords: Zigzag SiCNR; Melting range; Structural evolution; Melting point; Molecular dynamic simulation.

Classification numbers: 81.07.Nb.

I. INTRODUCTION

Two-dimensional (2D) materials have been the host of the topic since graphene was successfully synthesized by Andre Geim and Konstantin Novoselov. Although graphene possesses special physical properties (strong mechanical properties and high chemical and thermal stability), its disadvantage is the zero band gap [1–7]. Therefore, different types of 2D materials are studied to overcome the disadvantage of graphene, which can apply in electronic devices. Among these 2D materials, 2D-Xnene (silicene, germanene, stenene and so on) and their ligand-functionalized "Xane" derivatives play an important role in nanotechnology [8–14].

2D SiC is a semiconductor material created by the combination of Si and C atoms. 2D SiC has a large band gap of about 2.58 eV which is suitable for applications in many electronic devices [15–18]. Experimental synthesis of one-dimentional SiC structural forms was initiated by Hongjie Dai [19]. SiC nanorod was first synthesized by the interaction between carbon tubes and SiO. Later, series of techniques were developed for the synthesis of SiC wires such as sol – gel technique [20], vapor - liquid - solid technique [21], laser cutting technique [22], chemical vapor deposition [23]. Huan Zhang *et al.* reported that SiCNR had been successfully synthesized [24]. Following that, black Si powder and C powder were mixed horizontally in the furnace with the temperature from 1250˚C to 1500˚C for 5 to 12 hours in the atmosphere of Argon gas [24]. The results obtained SiCNR owned a length of 10 to 100 micrometres, a width of about 10 micrometres with a thickness of several nanometers [24].

In addition, theoretical studies of both zigzag SiCNR and armchair SiCNR are also focused on the electronic and mechanic properties. In terms of electronic properties, Lian Sun's team studied the relationship between electronic and magnetic properties of both zigzag and armchair types of SiCNR on the change of the band structure width [25]. The change in electronic properties was calculated using density functional theory while the magnetic change was calculated based on spin polarization [25]. The results showed that, for armchair SiCNR, the band gap width (about 2.36 eV) did not depend on the width of the ribbon. Armchair SiCNR was a non-magnetic semiconductor while zigzag SiCNR exhibited metallic properties.

In 2013, Alejandro et al. continued to study the semi-metallic properties of zigzag SiCNR as a premise for practice. They also used density function theory to study the property transition of zigzag SiCNR when adding O and S atoms to the zigzag edges [26]. They showed that the semi-metallic properties of the zigzag SiCNR changed to one of these cases: i) a metal when the O atoms were added to the zigzag edges; ii) a semiconductor if the S atoms were added. This shows the flexibility to change the properties of zigzag SiCNR in the devices. In addition, the elastic stress value of zigzag SiCNR (181 N/m) and that of armchair SiCNR (177 N/m) were calculated [27]. Especially, the doping SiCNRs with Boron and Nitrogen atoms also studied. C. D. Costa and J. M. Morbec used ab initio to study this association [28]. This study shows that impurities B and N did not affect the semiconductor properties of armchair SiCNR. The electronic properties of SiCNRs can be adjusted by doping B and N impurities into the lattice structure.

One can see that SiCNRs have attractive mechanical and electronic properties which are suitable for use in electronic devices. However, SiCNRs are also expected to become materials with exceptional thermal properties. Recently, in 2020, Sherajul Islam et al. calculated the thermal conductivity of both zigzag and armchair SiCNR by MD simulation method [29]. The conclusion of the study indicated that at 300 K, with the size 10 nm x 3 nm, the thermal conductivity of Armchair SiCNR was 23.92 ± 4.01 W/mK and Zigzag SiCNR was 26.6 ± 4.18 W/mK. Besides, the thermal conductivity of SiCNRs decreased with increasing length of the ribbon and vice versa, thermal conductivity increased with increasing the width of the ribbon.

Motivated by the recent experimental developments and theoretical investigations on SiCNR, in this paper we carried out a MD simulation in order to observe the evolution of the structure of SiCNR upon heating as well as the melting temperature and the information about the equilibrium phases at temperatures closed to and exceeding the melting point. Because of the limitation of the size and the high structural stability of SiCNR, it is difficult to study in experiments. Therefore, MD simulation is a suitable method that can be implemented. Details about the calculations are

showed in Sec. II. Results and discussions can be found in Sec. III. Conclusions are given in the last section of the paper.

II. CALCULATIONS

As for SiC, it is necessary to choose the suitable description of the interactions between Si and C, such as, covalent, ionic, Van de Waals and so on. Based on these reasons, a number of potentials have been studied, which can be mentioned as: Tersoff (1988) [30], PEF's energy potential of Eric Pearon (1984) [31], potential Modified Embedded-atom (1995) [32], and so on. Due to the empirical relevance of structure and the kinematic features, Vashishta interactive potentials are used to simulate the interaction between Si and C in this study. The Vashishta Interaction for SiC is performed based on the SiC binding characteristics by Priya Vashishta's team. This potential consists of four interactions: the spatially repulsive interaction due to the size of ions, the Coulomb interaction due to the charge transfer between ions, the dipole-charge interaction due to the electronic polarization of the ions, and interaction between the dipole – dipole [33]. The interaction energy of the system is given by the expression:

$$V = \sum_{i<j} V_{ij}^{(2)}(r_{ij}) + \sum_{i,j<k} V_{jik}^{(3)}(r_{ij}, r_{ik}) \tag{1}$$

The interaction energy expression between two objects shows the relationship between the four interactions mentioned above through the formula:

$$V_{ij}^{(2)}(r) = \frac{H_{ij}}{r^{\eta_{ij}}} + \frac{Z_i Z_j}{r} e^{-r/\lambda} - \frac{D_{ij}}{2r^4} e^{-r/\xi} - \frac{W_{ij}}{r^6}. \tag{2}$$

In which, H_{ij} is the magnitude of the spatial repulsion; Z_i, Z_j are effective charges of atoms i and j; D_{ij} is magnitude of the charge-dipole interaction; W_{ij} is magnitude of the dipole-dipole interaction; λ, ξ are parameters in the Coulomb interaction and the charge-dipole interaction.

However, because the interaction energy between two objects is not enough to properly describe SiC's properties. Therefore, interaction energy between the three bodies is required to exhibit structural changes in angles and edges during pressure and temperature changes, in particular,

$$V_{jik}^{(3)}(r_{ij}, r_{ik}) = R^{(3)}(r_{ij}, r_{ik}) P^{(3)}(\theta_{jik}), \tag{3}$$

$$R^{(3)}(r_{ij}, r_{ik}) = B_{jik} \exp(\frac{\gamma}{r_{ij} - r_0} + \frac{\gamma}{r_{ik} - r_0}) \times \Theta(r_0 - r_{ij})\Theta(r_0 - r_{ik}), \tag{4}$$

$$P^{(3)}(\theta_{jik}) = \frac{(\cos\theta_{jik} - \cos\overline{\theta}_{jik})^2}{1 + C_{jik}(\cos\theta_{jik} - \cos\overline{\theta}_{jik})^2}, \tag{5}$$

in which, B_{jik} is magnitude interaction; θ_{jik} is angle between r_{ij} and r_{ik}; $C_{jik}, \overline{\theta}_{jik}$ are constants.

To perform the calculations we use the Large-Scale Atomic/Molecular Massively Parallel Simulator (LAMMPS) software package which is designed to solve various problems by the methods of classical molecular dynamics [34].

The initial crystalline SiCNR model (Fig. 1) with 10000 atoms under periodic boundary conditions (PBCs) has been relaxed in the isothermal-isobaric ensemble (NPT) for 6×10^5 MD steps at $T_0 = 50K$. Note that one MD step takes 0.0001 picoseconds. Temperature T_i ($T_i = 5000K$) is chosen. It is higher than the melting point of free-standing graphene [35] or SiC to observe the
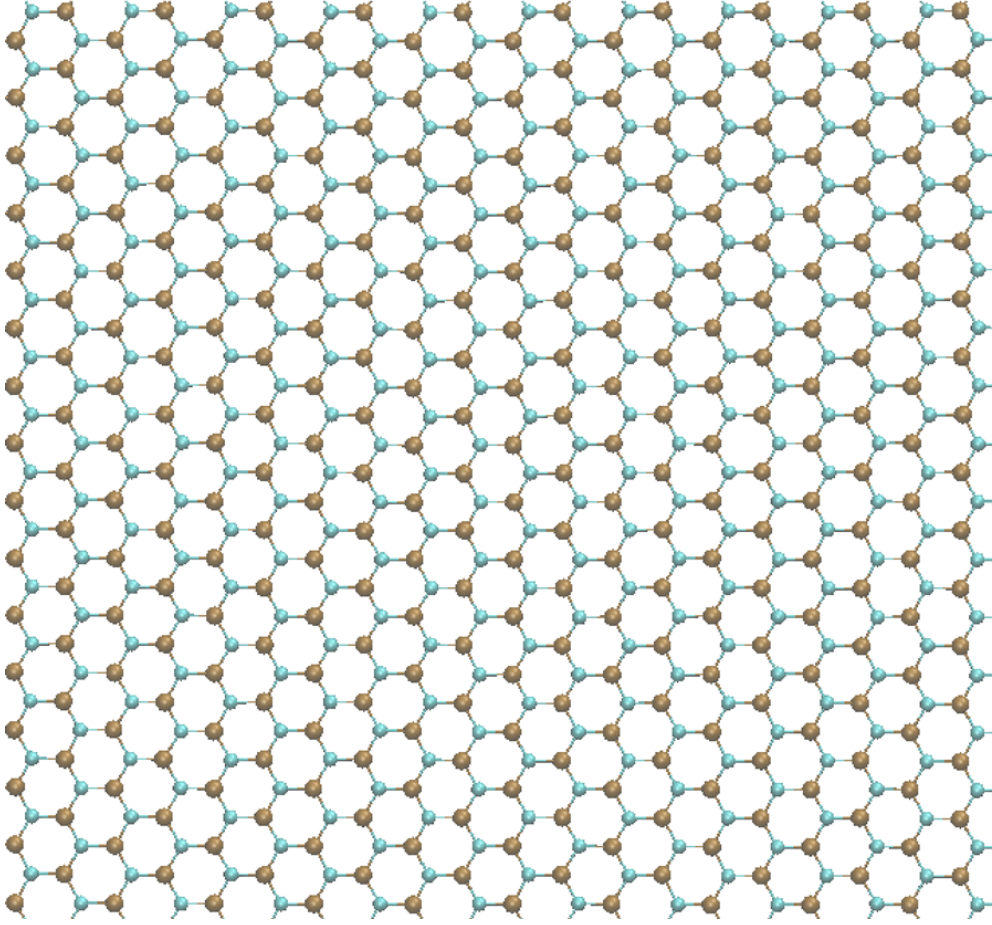
Fig. 1. The initial crystalline SiCNR model (536.1Å× 61.9Å) containing 10000 atoms.

evolution of the model upon heating. Then, the system is heated from the temperature T_0 to T_i. The heating rate is 10^{11} K/s.

We use the visual molecular dynamic (VMD) software (Illinois Univ.) for 2D visualization of atomic configurations. The temperature of the system is increased linearly via velocity rescaling as follows: $T = T_0 + \gamma t$ ($T_0 = 50K$, γ - heating rate, t - time required for heating). Models, obtained at each chosen temperature, have been relaxed at a given temperature for 6×10^5 MD steps before analyzing the structural characteristics or 2D visualization.

III. RESULTS AND DISCUSSION

The solid-liquid phase transition of zigzag SiCNR is observed by the graph showing the relationship between total energy per atom and temperature (the black square line in Fig. 2). The graph of the total energy per atom exhibits three temperature ranges, namely: from 50 K to 3500 K; from 3500 K to 4500 K; from 4500 K to 5000 K.

In the first stage (from 50 K to 3500 K) the total energy per atom increases linearly with the increase in temperature. This shows that, in this temperature range, the model remains in a solid state because the oscillation of the atoms in the model is very small around their equilibrium positions. At temperature of 3500 K, the oscillation amplitude of the atoms is large enough leading to break the atomic bonds in the lattice, resulting in the total energy per atom no longer obeying the linear law and increasing sharply from 3500 K to 4500 K. This means that the phase transition of zigzag SiCNR occurs in the temperature range from 3500 K to 4500 K. Therefore, the melting point of SiCNR can be found in this temperature range. In the final stage from 4500 K to 5000 K, the total energy continues to increase linearly, indicating that the model is in a liquid state.
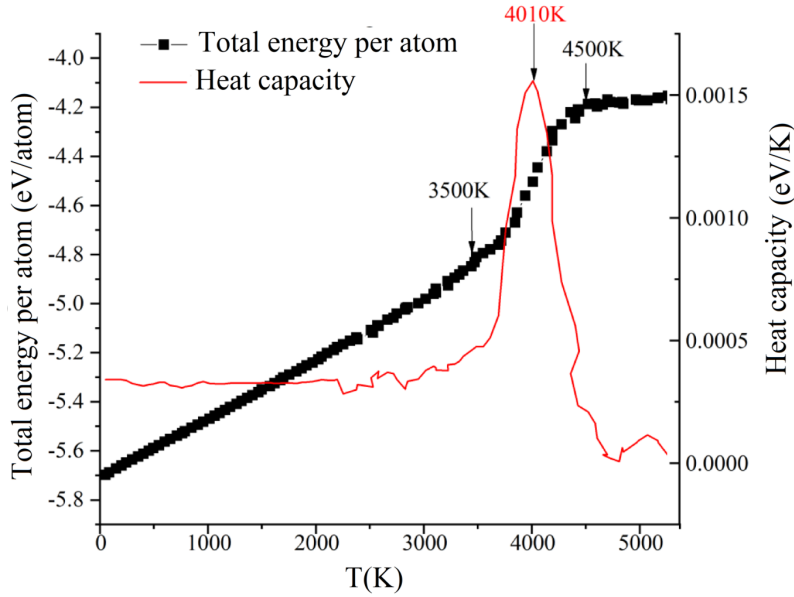

Fig. 2. The temperature dependence of the total energy per atom in the model (square line) and the heat capacity (solid line).

To accurately determine the melting temperature point of the model, it is necessary to base on the heat value of the model through the formula: $C_p = \frac{\Delta E}{\Delta T}$. Based on the graph of heat capacity on the temperature (solid line in Fig. 2), the heat capacity value below 3500 K is almost unchanged. This corresponds to a linear increase in the total energy per atom. However, from 3500 K to 4000 K, the value of heat capacity increases significantly because during this stage, the internal energy of the system increases sharply, causing breaking bonds to create atoms or clusters of atoms. It can be concluded that, from 3500 K to 4000 K, there exist both solid and liquid phases. Next, the heat capacity value peaks at 4010 K. Here, the energy of the system is maximized, breaking all the bonds leading to the initial model collapsing. Therefore, the melting temperature of zigzag SiCNR is determined in the vicinity of 4010 K. A snapshot of atomic structure at the melting state is presented in Fig. 3. Note that the melting point of monolayer SiC has not been measured experimentally yet, however, the melting point of free-standing SiC has defined at 4050 K using MD simulation [36]. After 4010 K, the model is in a liquid state, the heat
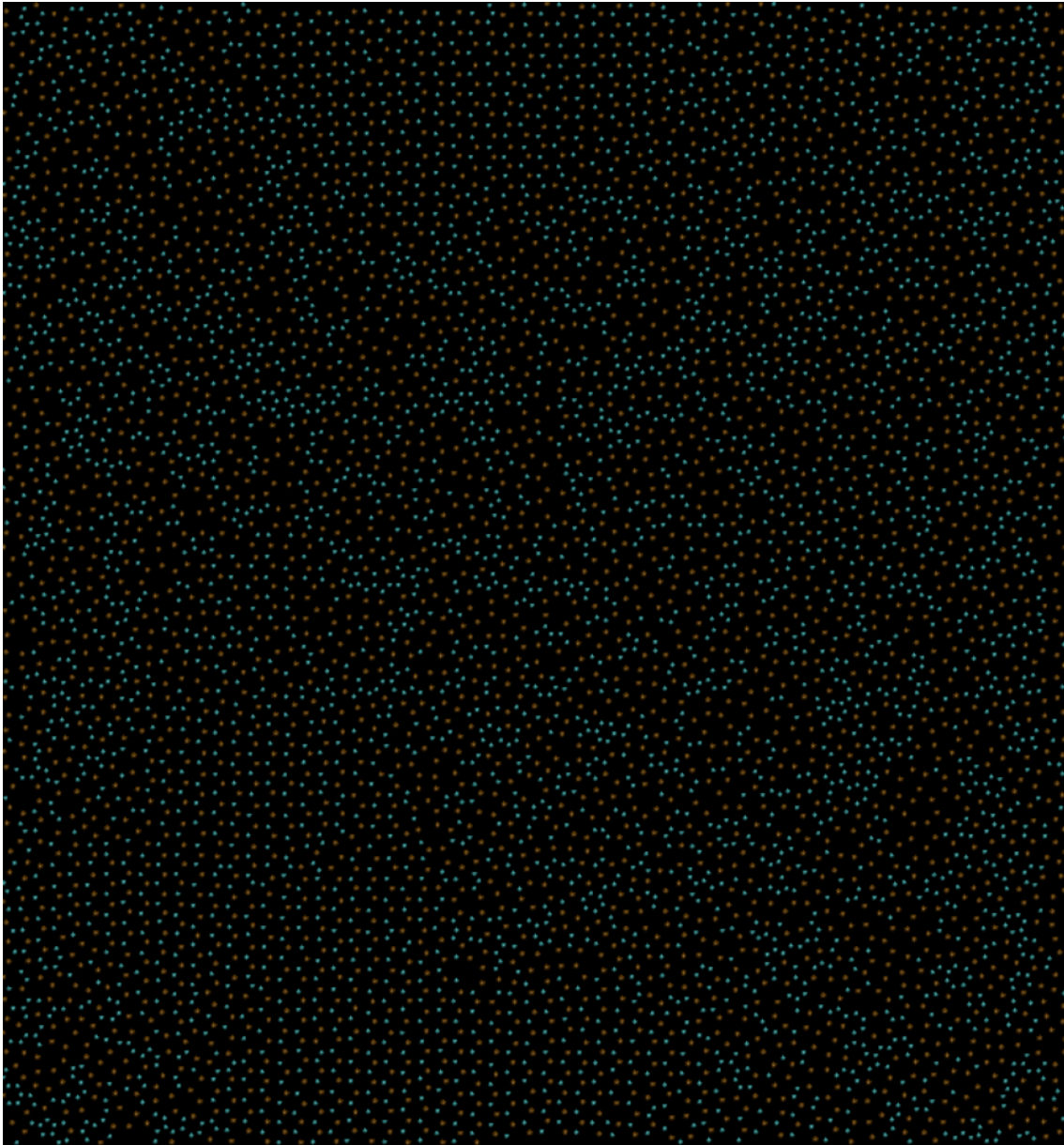
Fig. 3. The snapshots of atomic structures at the melting point of zigzag SiCNR.

capacity value changes slightly. Note that the structural evolution of Zigzag SiCNR upon heating are presented through radial distribution functions $g(r)$, coordinate number, angular distributions and ring distributions.

As well-known, the distributions of the atoms can be calculated using the radial distribution functions (Fig. 4). Note that the radial distribution functions denoted in equations by $g(r)$ defines
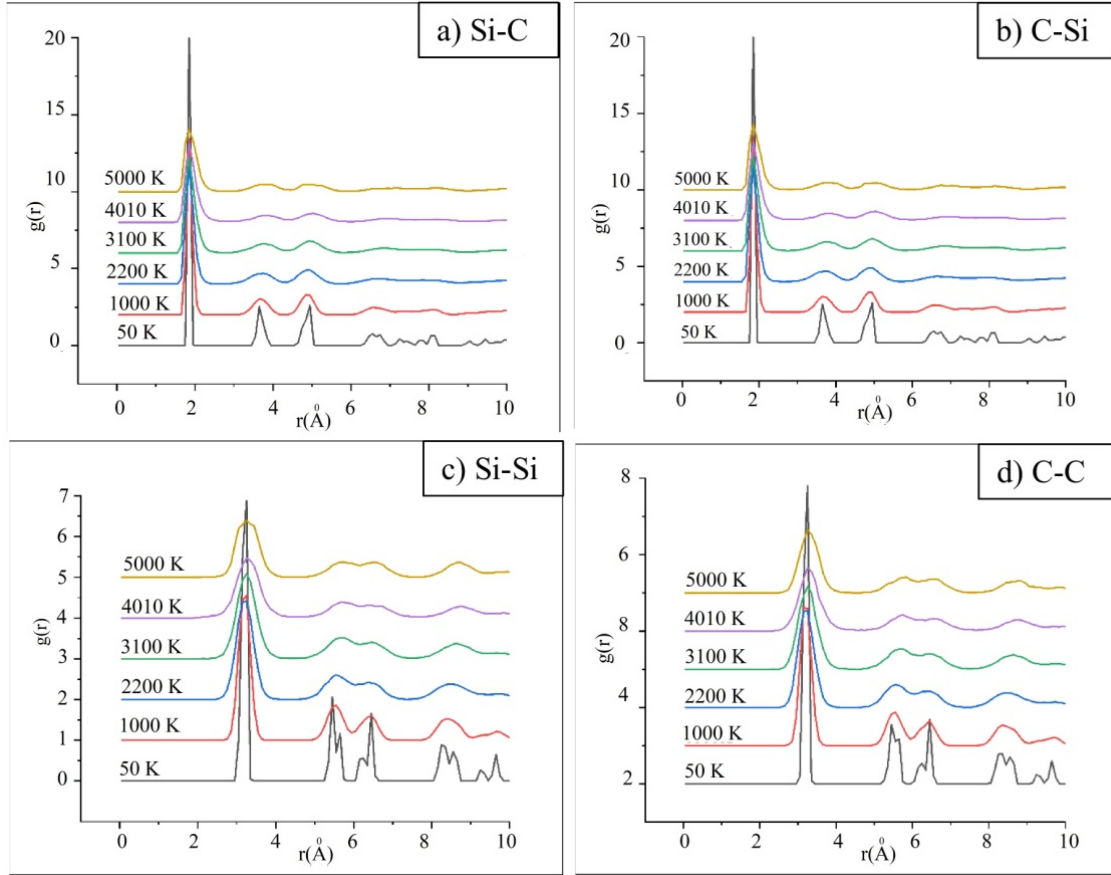
Fig. 4. Radial distribution function of zigzag SiCNR: a) Si-C; b) C-Si; c) Si-Si; d) C-C.

the probability of finding an atom at a distance r from another tagged atom [37]. The expression for g(r) is defined as follows:

$$g(r) = \frac{dn_r}{\rho 4\pi r^2 dr},\tag{6}$$

where, dn_r is a function that computes the number of atoms within a shell of thickness dr, the average density at any point is ρ.

In this work, the radial distribution functions are calculated for all atomic pairs: Si-C, C-Si, Si-Si, and C-C (Fig. 4). At temperature of 50 K, the graphs of all pairs with many peaks shows that the model is in a solid state (Fig. 4). The positions of the first peaks depend on each type of atomic pair that will have different cutoff radii. For this study, the positions of peaks of Si-C and C-Si pairs are around 1.9 Å (Figs. 4a, b) while the ones of Si-Si and C-C pairs are around 3.2 Å (Figs. 4c, 4d).

Then, as the temperature increases, the heights of the peaks decrease, indicating that there is a displacement of the atoms in the model leading to a change in density within the originally selected shear radius (1000 K-line, 2200 K-line, and 3100 K-line in Fig. 4). As for Si-C and C-Si

atomic pairs, at a temperature of 1000 K, the sharp peaks from r = 6 Å and further decrease significantly. These peaks completely disappeared in the temperature range from 2200 K to 3100 K. Related to Si-Si and C-C atomic pairs, all peak values from r = 5 Å decrease gradually. It means that Si and C atoms begin to have stronger oscillation amplitudes than the binding force between neighboring atoms, which changes the atomic density in the system. This indicates the beginning of the phase transition from solid to liquid states.

From the melting point of 4010 K and further, the first peaks of Si-C and C-S decrease significantly and the peaks between 3Å and 5.5Å are almost gone (4010 K-line and 5000 K-line in Figs. 4a, b). Whereas, the first peaks of Si-Si and C-C tend to be shorter and the remaining peaks fluctuate slightly (4010 K-line and 5000 K-line in Figs. 4c, d). Thus, the characteristic order structures of the crystal are broken and the model transforms into a liquid state.
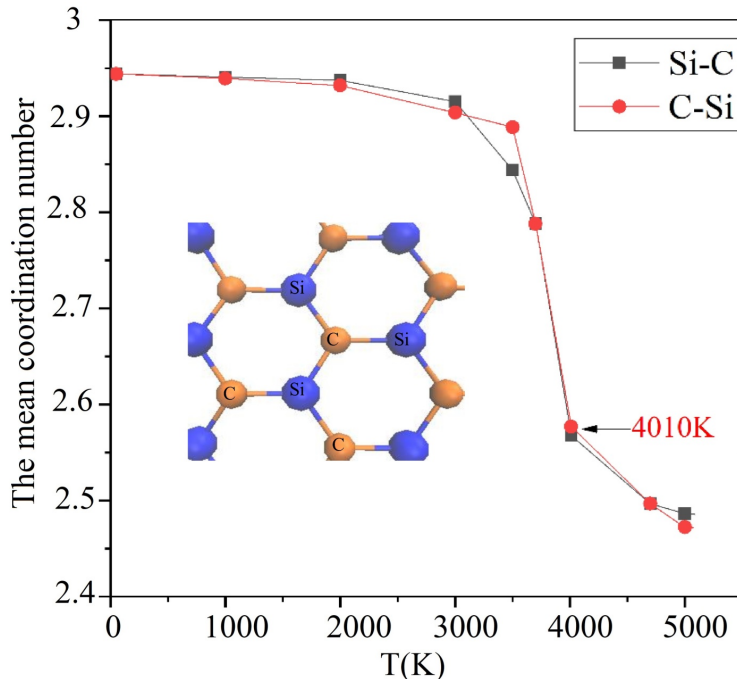

Fig. 5. The mean coordinate number of Si-C and C-Si atomic pairs with respect to temperature.

In crystallography, the coordination number describes the number of neighbor atoms with respect to a central atom [37]. Depending on the relative sizes of the central atom, the coordination number can vary from 2 to 16. In this study, if Si atom is taken as the central atom then there are three C atoms around Si atom in the closest positions, so the coordinate number of Si-C in a solid state is three (the inset in Fig. 5). In case, C atom is considered to be the central atom, there are three Si atoms around C atom in the closest positions (the inset in Fig. 5) and the coordinate number of C-Si in a solid state is also three.

In the present work, the mean coordination numbers of Si-C and C-Si are calculated to study the structural evolution of SiCNR upon heating (Fig. 5). At temperature 50 K, the model is in a solid state. However, the mean coordination numbers of Si-C and C-Si are a bit less than 3 (2.94) due to the existence of imperfect structure at the edges of the model. In the temperature range from 50 K to 3000 K, the mean coordination numbers of Si-C and C-Si are almost stable at 2.94 indicating that the model still exists in a solid state. In the temperature range from 3000 K to 3500 K, the mean coordination numbers of Si-C and C-Si decrease from 2.92 to 2.85 and from 2.91 to 2.88, respectively (Fig. 5). It means that the bonds of the atoms in the model are starting to break, causing the atoms to deviate from their original positions. From 3500 K to 4000 K, the mean coordination numbers of both Si-C and C-Si plummet and reach 2.57 at the melting point 4010 K. This indicates the phase transition of the model, the amplitude of the atoms is strong enough to break the initial bonds. Finally, from melting point and further temperature, the mean coordination number continues to decrease steadily, indicating that the pattern is in a liquid state.

In addition to the atomic mechanism of structural evolution of zigzag SiCNR, the ring distributions are studied. As well-known, the topological intermediate-range order can be characterized using a ring statistics algorithm which has been applied for all compositions from the rigorous investigation of networks generated using simulation [38].

In this work, the initial model exists in the form of six-fold ring as shown in the inset of Figure 5a because zigzag SiCNR has a hexagonal honeycomb structure. Upon heating, the ring distributions are calculated at some given temperatures (Fig. 6). At 50 K, the hexagonal ring form accounts for 100% because the model is in a solid state (Fig. 6a). Up to 3500 K, there is a slight decrease of six-fold ring to 95% while other rings appear, such as, three-fold, four-fold, five-fold, eight-fold, and ten-fold rings (Fig. 6b). Because temperature energizes some of the vibrating atoms, this oscillation breaks some bonds to form new rings. At the melting point of 4010 K, a sharp decrease in the six-fold ring to almost 40% and a rapid increase in the three-fold ring (nearly 70%) (Fig. 6c). This indicates that the increase in the thermal motion of the atoms affects the ring structural bonds and disrupts the structure of the original lattice. Finally, at 5000 K, the three-fold ring ratio continues to increase while the six-fold ring ratio continues to decrease showing that the pattern forms multiple clusters that are scattered in space, creating a liquid body (Fig. 6d).

During heating process, there could be structures with 3-coordinate number and six-fold ring but not hexagonal structures. Therefore, to investigate these distorted structures, the angular distribution is one of the optimal choices to contribute to the mechanism of structural evolution of zigzag SiCNR (Fig. 7).

At 50 K, the angular distribution ratio of Si-C-Si and C-Si-C range from $115°$ to $125°$ and peak at $120°$ because the atoms are ordered in the lattice (Fig. 7). From 2000 K to the melting point of 4010 K, there is a sharp decrease in the $120°$ angle distributions. It can be seen that the atoms in the model are vibrating vigorously around the initial equilibrium positions, causing the bond angle between the atoms deflected, ranging from $85°$ to $150°$. One can conclude that in this temperature range, many distorted structures exists. At 5000 K, the $120°$ angle distributions continue to decrease. In addition, the formation of additional small peaks between $70°$ and $175°$ indicate that the atom clusters have broken out of the lattice to form smaller angles and the model is in a liquid state.
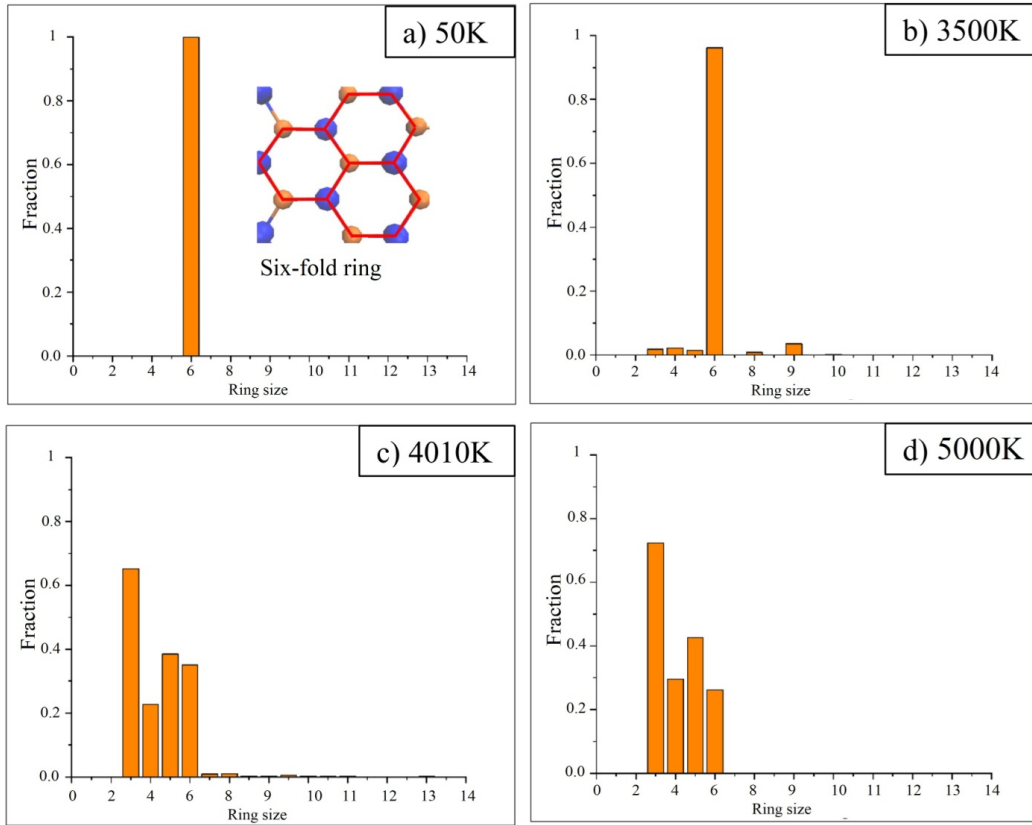
Fig. 6. The ring distributions of zigzag SiCNR: a) 50 K; b) 3500 K; c) 4010 K; d) 5000 K.
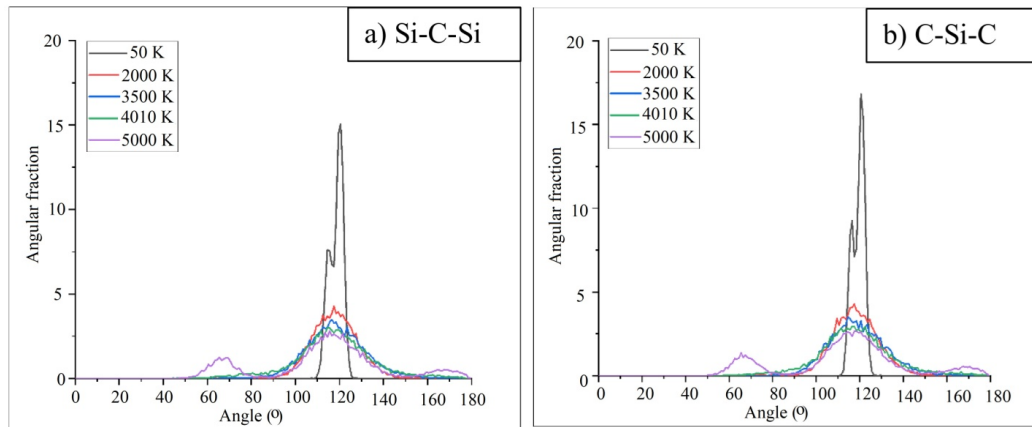

Fig. 7. The angle distributions of zigzag SiCNR at given temperatures: a) Si-C-Si; b) C-Si-C.

IV. CONCLUSIONS

In this study, zigzag SiCNR is studied via molecular dynamics simulation. The initial model contained 10000 atoms are studied via Vashishta potentials to have an entire picture about the structural evolution of zigzag SiCNR upon heating. The melting temperature range is defined from 3500 K to 4500 K based on the total energy per atom. The melting point of zigzag SiCNR is calculated using the heat capacity and defined at 4010 K. This point of temperature (4010 K) is close to the one of free-standing SiC (4050K). The mechanism of structural evolution upon heating is presented: the peaks of the radial distribution functions tend to decrease gradually and to be smooth at the melting point; the mean coordinate number of Si-C and C-Si decreased from 2.94 to 2.45; the six-fold ring of the initial model is converted to different ring sizes; the ratio angle distribution at 120° decreases leading to the formation of distorted structures.

ACKNOWLEDGEMENTS

REFERENCES

[1] Y. Matsumoto, G. Hirata, H. Takakura, H. Okamoto, and Y. Hamakawa, *A new type of high efficiency with a low-cost solar cell having the structure of a* μ *c-SiC/polycrystalline silicon heterojunction*, J. Appl. Phys. **67** (1990) 6538.

[2] K.S. Novoselov, A. K. Geim, S.V. Morozov, D. Jiang, M.I. Katsnelson, I. Grigorieva, S. Dubonos and A. A. Firsov, *Two-dimensional gas of massless Dirac fermions in graphene*, Nature **438** (2005) 197.

[3] Y. Zhang, Z. Jiang, J. Small, M. Purewal, Y.-W. Tan, M. Fazlollahi, J. Chudow, J. Jaszczak, H. Stormer, and P. Kim, *Landau-level splitting in graphene in high magnetic fields*, Phys. Rev. Lett. **96** (2006) 136806.

[4] P. Blake, E. Hill, A. Castro Neto, K. Novoselov, D. Jiang, R. Yang, T. Booth, and A. Geim, *Making graphene visible*, Appl. Phys. Lett. **91** (2007) 063124.

[5] I. Meric, M.Y. Han, A.F. Young, B. Ozyilmaz, P. Kim, and K. L. Shepard, *Current saturation in zero-bandgap, top-gated graphene field-effect transistors*, Nat. Nanotechnol. **3** (2008) 654.

[6] W. L. Wang, S. Meng, and E. Kaxiras, *Graphene nanoflakes with large spin*, Nano Lett. **8** (2008) 241.

[7] D. R. Cooper, B. D'Anjou, N. Ghattamaneni, B. Harack, M. Hilke, A. Horth, N. Majlis, M. Massicotte, L. Vandsburger, and E. Whiteway, *Experimental review of graphene*, Int. Sch. Res. Notices **2012** (2012) 501686.

[8] D.-Q. Fang, S.-L. Zhang, and H. Xu, *Tuning the electronic and magnetic properties of zigzag silicene nanoribbons by edge hydrogenation and doping*, RSC Adv. **3** (2013) 24075.

[9] L. Matthes and F. Bechstedt, *Influence of edge and field effects on topological states of germanene nanoribbons from self-consistent calculations*, Phys. Rev. B, **90** (2014) 165431.

[10] Y. Du, H. Liu, B. Xu, L. Sheng, J. Yin, C.-G. Duan, and X. Wan, *Unexpected magnetic semiconductor behavior in zigzag phosphorene nanoribbons driven by half-filled one dimensional band*, Sci. Rep. **5** (2015) 1.

[11] T.-C. Wang, C.-H. Hsu, Z.-Q. Huang, F.-C. Chuang, W.-S. Su and G.-Y. Guo, *Tunable magnetic states on the zigzag edges of hydrogenated and halogenated group-IV nanoribbons*, Sci. Rep. **6** (2016) 1.

[12] E. G. Marin, D. Marian, G. Iannaccone and G. Fiori, *First principles investigation of tunnel FETs based on nanoribbons from topological two-dimensional materials*, Nanoscale **9** (2017) 19390.

[13] M. Monshi, S. Aghaei and I. Calizo, *Edge functionalized germanene nanoribbons: impact on electronic and magnetic properties*, RSC Adv. **7** (2017) 18900.

[14] C. Chen, B. Huang and J. Wu, Be_3N_2 *monolayer: A graphene-like two-dimensional material and its derivative nanoribbons*, AIP Adv. **8** (2018) 105105.

[15] E. Bekaroglu, M. Topsakal, S. Cahangirov and S. Ciraci, *First-principles study of defects and adatoms in silicon carbide honeycomb structures*, Phys. Rev. B, **81** (2010) 075433.

[16] S. Lin, *Light-emitting two-dimensional ultrathin silicon carbide*, J. Phys. Chem. C **116** (2012) 3951.

[17] Z. Shi, Z. Zhang, A. Kutana and B.I. Yakobson, *Predicting two-dimensional silicon carbide monolayers*, *ACS nano* **9** (2015) 9802.

[18] T. Susi, V. Skákalová, A. Mittelberger, P. Kotrusz, M. Hulman, T. J. Pennycook, C. Mangler, J. Kotakoski, and J. C. Meyer, *Computational insights and the observation of SiC nanograin assembly: towards 2D silicon carbide*, *Sci. Rep.* **7** (2017) 1.

[19] H. Dai, E. W. Wong, Y. Z. Lu, S. Fan and C. M. Lieber, *Synthesis and characterization of carbide nanorods*, *Nature* **375** (1995) 769.

[20] G. Meng, L. Zhang, C. Mo, S. Zhang, Y. Qin, S. Feng and H. Li, *Preparation of β–SiC nanorods with and without amorphous SiO2 wrapping layers*, *J. Mater. Res.* **13** (1998) 2533.

[21] S. Deng, Z. Wu, J. Zhou, N. Xu, J. Chen and J. Chen, *Synthesis of silicon carbide nanowires in a catalyst-assisted process*, *Chem. Phys. Lett.* **356** (2002) 511.

[22] W. Shi, Y. Zheng, H. Peng, N. Wang, C.S. Lee and S.T. Lee, *Laser ablation synthesis and optical characterization of silicon carbide nanowires*, *J. Am. Ceram. Soc.* **83** (2000) 3228.

[23] J. Wei, K.-Z. Li, H.-J. Li, Q.-G. Fu and L. Zhang, *Growth and morphology of one-dimensional SiC nanostructures without catalyst assistant*, *Mater. Chem. Phys.* **95** (2006) 140.

[24] H. Zhang, W. Ding, K. He and M. Li, *Synthesis and characterization of crystalline silicon carbide nanoribbons*, *Nanoscale Res. Lett.* **5** (2010) 1264.

[25] L. Sun, Y. Li, Z. Li, Q. Li, Z. Zhou, Z. Chen, J. Yang and J. Hou, *Electronic structures of SiC nanoribbons*, *J. Chem. Phys.* **129** (2008) 174114.

[26] A. Lopez-Bezanilla, J. Huang, P. R. Kent and B. G. Sumpter, *Tuning from half-metallic to semiconducting behavior in sic nanoribbons*, *J. Phys. Chem. C* **117** (2013) 15447.

[27] D.-T. Nguyen and M.-Q. Le, *Mechanical properties of various two-dimensional silicon carbide sheets: An atomistic study*, *Superlattices Microstruct.* **98** (2016) 102.

[28] C. Costa and J. Morbec, *Boron and nitrogen impurities in SiC nanoribbons: an ab initio investigation*, *J. Phys.: Condens. Matter.* **23** (2011) 205504.

[29] M. S. Islam, A. J. Islam, O. Mahamud, A. Saha, N. Ferdous, J. Park and A. Hashimoto, *Molecular dynamics study of thermal transport in single-layer silicon carbide nanoribbons*, *AIP Adv.* **10** (2020) 015117.

[30] J. Tersoff, *Modeling solid-state chemistry: Interatomic potentials for multicomponent systems*, *Phys. Rev. B* **39** (1989) 5566.

[31] E. Pearson, T. Takai, T. Halicioglu, and W.A. Tiller, *Computer modeling of Si and SiC surfaces and surface processes relevant to crystal growth from the vapor*, *J. Crys. Growth* **70** (1984) 33.

[32] M.I. Baskes, *Determination of modified embedded atom method parameters for nickel*, *Mater. Chem. Phys.* **50** (1997) 152.

[33] P. Vashishta, R.K. Kalia, A. Nakano and J. P. Rino, *Interaction potential for silicon carbide: A molecular dynamics study of elastic constants and vibrational density of states for crystalline and amorphous silicon carbide*, *J. Appl. Phys.* **101** (2007) 103515.

[34] S. J. Plimpton and A. P. Thompson, *Computational aspects of many-body potentials*, *MRS Bull.* **37** (2012) 513.

[35] V. V. Hoang, L. T. Cam Tuyen, and T. Q. Dong, *Stages of melting of graphene model in two-dimensional space*, *Philos. Mag.* **96** (2016) 1993.

[36] T. M. Le Nguyen, V. Van Hoang, and H. T. Nguyen, *Structural evolution of free-standing 2D silicon carbide upon heating*, *Eur. Phys. J. D* **74** (2020) 1.

[37] J. L. Finney, *Bernal's road to random packing and the structure of liquids*, *Philos. Mag.* **93** (2013) 3940.

[38] S. Le Roux and P. Jund, *Ring statistics analysis of topological networks: New approach and application to amorphous GeS2 and SiO2 systems*, *Comput. Mater. Sci.* **49** (2010) 70.